Stanford Exploration Project, Report 113, July 8, 2003, pages 85–96

Short Note

Prestack time imaging operator for 2-D and 3-D pegleg multiples over nonflat geology

Morgan Brown[1]

INTRODUCTION

My Least-squares Joint Imaging of Multiples and Primaries (LSJIMP) algorithm (Brown, 2003b) separates pegleg multiples and primaries. LSJIMP computes separate images of the peglegs and primaries, and then uses the mutual consistency of the images to discriminate against unwanted noise types in each image. The images must be consistent in two respects: kinematics and amplitudes. A companion paper (Brown, 2003a) paper addresses the amplitude issue. In this paper, I address the kinematics. Kinematically, the events must be correctly positioned in time and flat with offset. To this end, I derive new time imaging operator, "HEMNO" (Heterogeneous Earth Multiple NMO Operator).

To correctly image primary or multiple reflections in a heterogeneous earth, migration reigns supreme, although its computational cost may be nontrivial over complex geology, in 3-D, or when a "true amplitude" image is required. My previously presented (Brown, 2002a) joint imaging technique used normal moveout (NMO), because of NMO's speed and its amplitude predictability, despite its inability to account for nonflat geology. HEMNO correctly accounts for moderate subsurface structure but retains the speed and amplitude advantages of NMO. I show that the 2-D and 3-D pegleg moveout equations for two dipping planes derived by Levin and Shah (1977) and Ross et al. (1999), respectively, reduce to HEMNO in the small dip angle limit.

When used in conjunction with LSJIMP, I show that HEMNO produces improved results on the moderately complex Mississippi Canyon 2-D multiples test dataset, relative to a flat-earth NMO operator. Nevertheless, the real value of HEMNO lies in 3-D. Guitton (2003) demonstrates that the "Delft method" (Verschuur et al., 1992) (plus advanced multiple subtraction technology), almost perfectly separates surface-related multiples from 2-D data with complex 2-D structure. However, in real-world 3-D situations, acquisition and computational constraints diminish the method's applicability. I demonstrate that in a simple, yet realistic, 3-D synthetic example that HEMNO can accurately image pegleg multiples from a seabed that dips in both directions. In the future, HEMNO should prove a useful advance in 3-D multiple separation.

[1]**email:** morgan@sep.stanford.edu

TRAVELTIME EQUATION FOR PEGLEG MULTIPLES IN A NON-FLAT EARTH

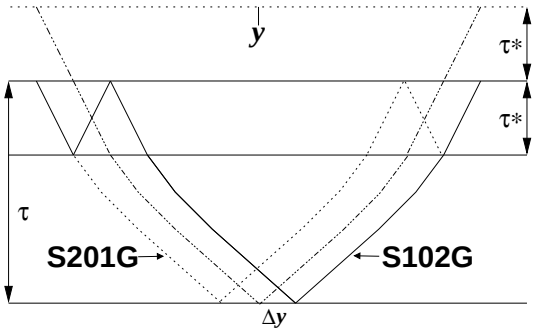

Figure 1: NMO for multiples in a 1-D earth. Pegleg multiples "S201G" and "S102G" have the same traveltimes as "pseudo-primary" with the same offset and an extra zero-offset traveltime τ^*, given the velocity and time-thickness of the top layer. morgan1-schem [NR]

A first-order pegleg multiple consists of two unique arrivals: the event with a multiple bounce over the source, and the event with a bounce over the receiver. Figure 1 shows that in a flat earth, both "legs" of a pegleg (denoted S102G and S201G) arrive simultaneously; when the reflector geometry varies with position, they generally do not. In some cases, pegleg multiples are actually observed to "split", though humans rarely observe the phenomenon unambiguously in field data, unless the reflector geometry is uniformly dipping over a large distance (see (Morley, 1982), for a good example).

The practical non-observation of split peglegs notwithstanding, geologic heterogeneity is a first-order effect in the accurate modeling of their kinematic and amplitude behavior. Mild variations in reflector depth over a cable length can introduce significant destructive interference between the legs of a pegleg multiple at far offsets – interference impossible to predict with a 1-D theory.

Levin and Shah (1977) deduced analytic kinematic moveout equations for 2-D pegleg multiples arising from two dipping layers, and Ross et al. (1999) extended the work to 3-D. Both approaches assume constant velocity and locally planar reflectors – assumptions which, depending on local geology, may be unrealistic in practice. In this section, I present "HEMNO" (short for Heterogeneous Earth Multiple NMO Operator), a simplified moveout equation based upon a more practically realizable conceptual model. In Appendix A, I show that the HEMNO equation is equivalent to Levin and Shah's in the limit of small dip angle.

Brown (2002a) derived an extension to the conventional NMO equation which images pegleg multiples at the zero-offset traveltime of the target reflector:

$$t = \sqrt{(\tau + j\tau^*)^2 + x^2/V_{eff}^2}. \tag{1}$$

$j\tau^*$ is the two-way traveltime of a j^{th}-order pegleg in the multiple-generating layer. $V_{eff}(\tau)$ is the effective RMS velocity of the equivalent primary shown in Figure 1.

$$V_{eff}(\tau) = \left(j\tau^* V^*(\tau^*) + \tau V(\tau)\right) / \left(j\tau^* + \tau\right) \tag{2}$$

Figure 2 graphically illustrates HEMNO in a constant-velocity earth. The solid line in panel d) is the final result. It has the equation of a hyperbola with zero-offset traveltime $\tau^*(y_0 -$

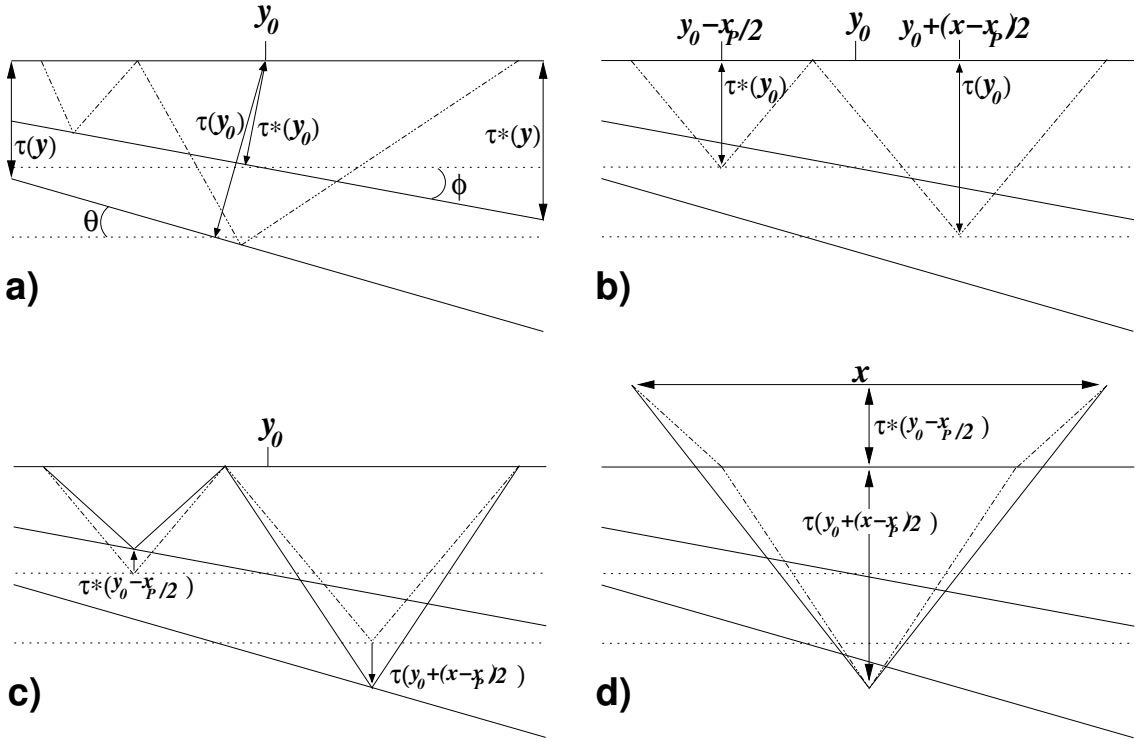

Figure 2: Raypath for single-CMP approximate imaging operator. Panel a): True raypath in constant-velocity earth. The zero-offset traveltimes to the seabed and subsea reflector are $\tau^*(y_0)$ and $\tau(y_0)$, respectively. Panel b): Assumed reflection points under flat-earth assumption. x_p is defined in equation (4). Panel c): The appoximation. Stretch legs of raypath vertically to match measured $\tau^*(y_0 - x_p/2)$ and $\tau(y_0 + (x - x_p)/2)$. Panel d): Final step. Connect legs of raypath. The solid line that connects the reassembled raypath is the final result. morgan1-schem-pegleg-dip2 [NR]

$x_p/2) + \tau(y_0 + (x - x_p)/2)$ and the same offset, x:

$$t^2 = \left[\tau(y_0 - (x - x_p)/2) + \tau^*(y_0 - x_p/2)\right]^2 + \frac{x^2}{V_{eff}^2} \tag{3}$$

The following expression for x_p, the width of the pegleg's primary leg in an assumed 1-D earth, is derived in (Brown, 2003a).

$$x_p^2 = \frac{x^2 \tau^2 V^4}{(\tau + j\tau^*)^2 V_{eff}^4 + x^2 (V_{eff}^2 - V^2)} \tag{4}$$

Although equation (3) was derived by seemingly *ad hoc* means, I show in Appendix A that the HEMNO raypath is a first-order approximation of Levin and Shah's (1977) true raypath. The V_{eff} shown in equation (3) is modified relative to that in equation (2); $\tau^*(y_0 - x_p/2)$ is substituted for τ^* and $\tau(y_0 - (x - x_p)/2)$ is substituted for τ.

Practical implementation of the HEMNO equation

To implement equation (3) on a computer, we must obtain two quantities. The first, the zero-offset traveltime of the seabed, $\tau^*(y)$, may be obtained by hand- or auto-picking. Unfortunately, the second quantity, the zero-offset traveltime to an arbitrary subsea reflector at $y = y_0 \pm (x - x_p)/2$, cannot realistically be picked. Panel c) of Figure 2 motivates the problem; starting at $\tau(y_0)$, the subsea reflector must be followed to $y = y_0 + (x - x_p)/2$. My approach to the problem is similar to Lomask and Claerbout's (2002) algorithm for automatically flattening seismic data. It requires a smooth, unambiguous estimate of reflector dip. I summarize this approach (in 2-D; extension to 3-D is more involved but conceptually similar) in pseudocode:

Obtain zero offset section, $\mathbf{d}(\tau, y)$, by stacking input data.
Use $\mathbf{d}(\tau, y)$ to compute smooth reflector dip, $\mathbf{p}(\tau, y)$, using technique of Fomel (2002).
Set $k = 1$, $y = y_0$.
do while $\left(y + \Delta y \le y_0 + (x - x_p)/2 \right)$
  Set $y = y_0 + (k-1)\Delta y$
  Set $\tau(y + \Delta y) = \tau(y + \Delta y) + \mathbf{p}(\tau(y), y)$
  Set $k = k + 1$
end do

This approach suffers from some possible pitfalls.

- In the "τ^* to $2\tau^*$ zone", $\mathbf{d}(\tau, y)$ consists of primary events only, and to a (normally) lesser extent, other coherent noise modes (e.g. locally-converted shear waves, internal multiples). For $\tau > 2\tau^*$, $\mathbf{d}(\tau, y)$ contains both peglegs and primaries, as well as other possibly strong unmodeled multiple reflection modes, and the dip of these events is unlikely to be equal.

  Previous authors (Fomel, 2001; Brown, 2002b) have developed methods to simultaneously estimate two crossing dips. The problem is inherently nonlinear, and thus highly dependent on initial guesses for the two dips. Assuming weak non-primary/pegleg noise, a possible strategy might be to seed the pegleg dip with primary dip from above.

  In current implementation, however, I ignore this problem by setting the dip to zero in the $\tau > 2\tau^*$ zone. I justify this assumption by noting that as τ increases, the distance from y_0 to $y_0 \pm (x - x_p)/2$ shrinks asmyptotically to zero, so unless the reflector dip is severe (inconsistent with the derivation of equation(3)), this omission will not present a large problem.

- Faults and other event discontinuities in $\mathbf{d}(\tau, y)$ are inconsistent with the "smooth" $\mathbf{p}(\tau, y)$ mentioned above. The current implementation ignores any possible faulting, although the dip estimation algorithm used can handle steeply folding reflectors.

EXAMPLES

In 1997, WesternGeco distributed a 2-D test dataset, acquired in the Mississippi Canyon region of the Gulf of Mexico, for the testing of multiple suppression algorithms. The data contain a variety of strong surface-related multiples, and enough geologic complexity to render one-dimensional methods ineffectual. Figure 3 shows the stack of the raw data.

Figures 4 and 5 illustrate the superior performance of the HEMNO operator versus 1-D NMO when used in LSJIMP. This figure is shown in better context in Brown (2003b). The strong top of salt seabed pegleg in Figure 4, dipping over this midpoint range, is clearly better removed when HEMNO is used. Figure 5 illustrates a more insidious problem: because the 1-D NMO operator did not focus a pegleg at the correct time, it caused a spurious event to be manufactured at a slightly smaller time.

Figure 6 compare the results of LSJIMP at a single midpoint (0 m), with and without HEMNO. The differences are fairly subtle, but illustrative. Although the dip in this region is mild, it is strong enough to cause the R1 pegleg multiple with $\tau = 4$ sec to defocus at far offsets. The thinly layered reflection is particularly susceptible to destructive interference with dip. On the center row of the figure, notice that in the HEMNO result, the defocusing effect is modeled, while in the 1-D result it is not. The difference panel further shows that HEMNO better models this effect.

Figure 7 illustrates the HEMNO operator applied to a synthetic 3-D dataset. The dataset consists of a seabed reflection and multiples only, with constant velocity and inline and crossline dips of 4° and 2°, respectively. Figure 7 shows a near-offset section after conventional NMO (left) and HEMNO for first-order multiples (right). The seabed multiple doesn't "split", but it is nontheless treated as a pegleg by HEMNO, so this example does test HEMNO's effectiveness in 3-D. Notice that over the entire survey area, the multiple and primary are mutually focused.

CONCLUSIONS

I introduced a new time-imaging operator for pegleg multiples, called HEMNO. HEMNO operates on single CMP gathers, making it computationally efficient and predictable in terms of amplitude behavior. I demonstrate that HEMNO can correctly account for moderate variation in reflector geometry with position, and that in a joint imaging context (LSJIMP), HEMNO accurately models both the vertical positioning of peglegs and some of the focusing effects with offset.

ACKNOWLEDGMENT

WesternGeco acquired and released the Mississippi Canyon dataset for public use.

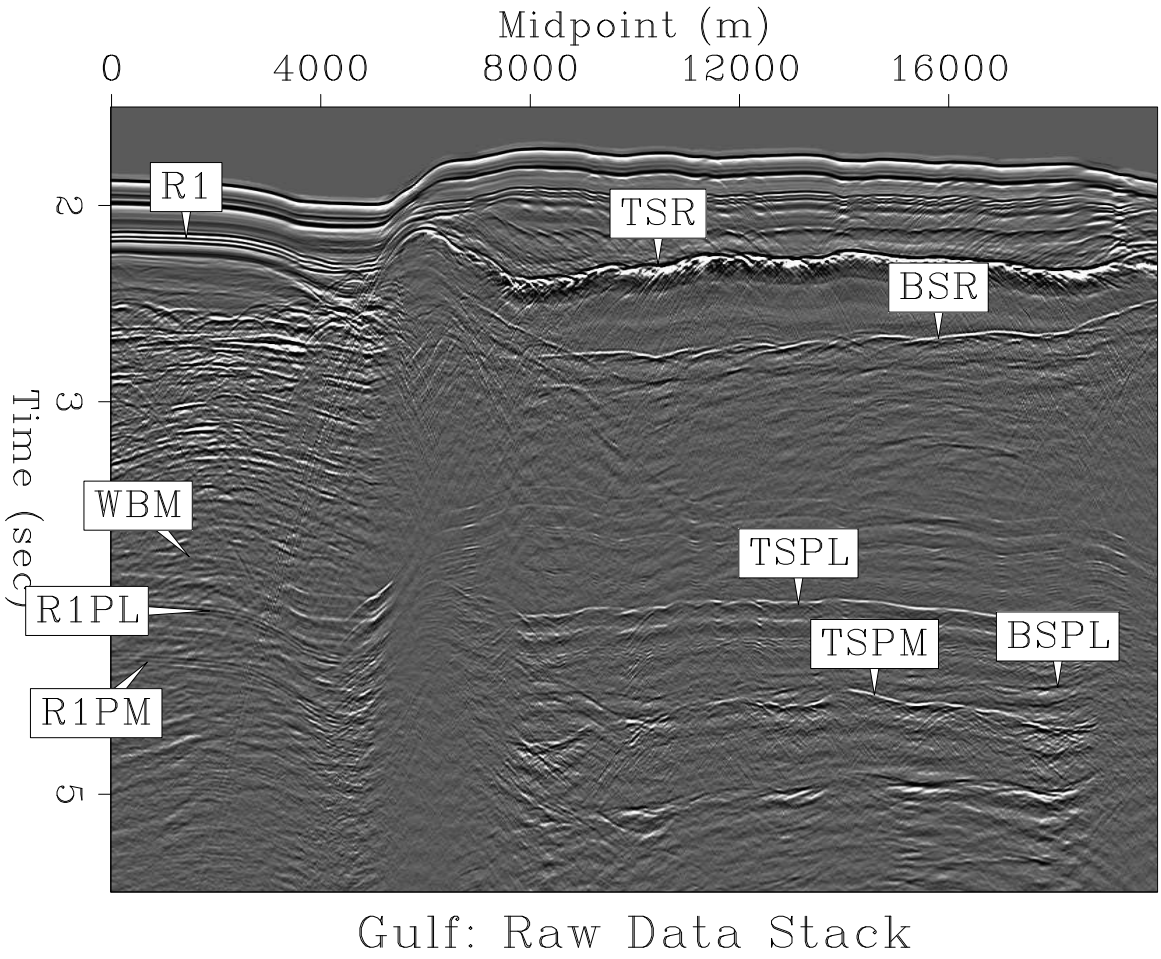

Figure 3: Stacked Mississippi Canyon 2-D dataset (750 midpoints), annotated with important horizons and multiples. Labeled events: R1 - strong reflection; TSR - top of salt; BSR - bottom of salt; WBM - first seabed multiple; R1PL - seabed pegleg of R1; R1PM - R1 pure surface multiple; TSPL - seabed pegleg of TSR; BSPL - seabed pegleg of BSR; TSPM - TSR pure surface multiple. morgan1-gulf.stackraw [CR]

APPENDIX A

Proof of Equivalence with Levin and Shah's Traveltime Equations for Small Dips

In the following appendix, I show in that the approximate traveltime equation for pegleg multiples in a nonflat earth, equation (3), is a valid first-order approximation of Levin and Shah's (1977) true raypath.

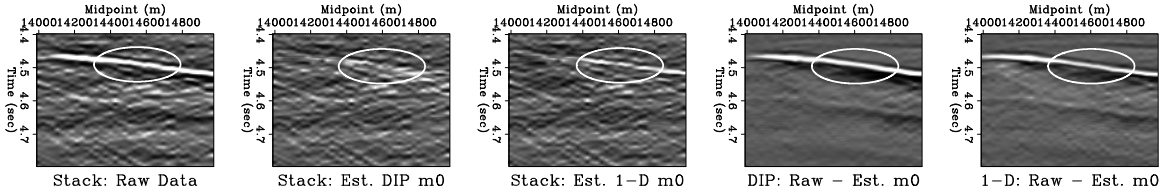

Figure 4: LSJIMP stack comparison of HEMNO versus 1-D NMO operator. All panels windowed from 4.4 to 4.8 seconds in time; 14000 to 15000 meters in midpoint. From L to R: Raw data stack; Stack of estimated $\mathbf{m}_0$ using HEMNO; Stack of estimated $\mathbf{m}_0$ using 1-D NMO operator; HEMNO difference; 1-D NMO difference. Seabed pegleg from top of salt reflection is outlined in all panels. morgan1-stackcomp-dipcomp.1.gulf [CR]

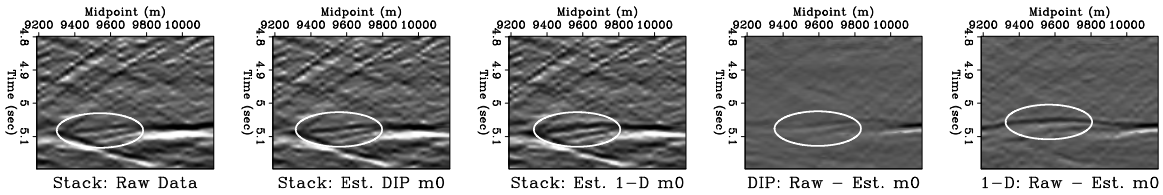

Figure 5: LSJIMP stack comparison of HEMNO versus 1-D NMO operator. All panels windowed from 4.8 to 5.2 seconds in time; 9200 to 10200 meters in midpoint. From L to R: Raw data stack; Stack of estimated $\mathbf{m}_0$ using HEMNO; Stack of estimated $\mathbf{m}_0$ using 1-D NMO operator; HEMNO difference; 1-D NMO difference. The ovals highlight a nonexistent event "removed" from data due to 1-D NMO's inferior performance over nonflat structure. morgan1-stackcomp-dipcomp.2.gulf [CR]

Levin and Shah's Traveltime Equations

Levin and Shah (1977) show that for a flat subsea reflector and dipping seabed, the moveout equation of the "S102G" (source-seabed-surface-reflector-receiver) pegleg multiple is:

$$(tV)^2 = \left[\tau^* \cos\theta + \tau \cos\phi\right]^2 + \left[\frac{x\cos(\phi+\theta)}{V} - \tau^* V \sin\theta - \tau V \sin\phi\right]^2, \qquad \text{(A-1)}$$

where ϕ and θ are the dip angle (in radians) of the seabed and subsea reflector, respectively. For small dip angles (i.e., less than 5 degrees), we can make the small angle approximation for angles ϕ, θ, and $\phi+\theta$ to update equation (A-1) accordingly:

$$(tV)^2 = \left[\tau^* + \tau\right]^2 + \left[x - \tau^* V\theta - \tau V\phi\right]^2. \qquad \text{(A-2)}$$

Multiplying out the squares in equation (A-2) and collecting terms gives:

$$t^2 = \left[\tau^* + \tau\right]^2 + \frac{x^2}{V^2} - 2\frac{\theta\tau^* x}{V} - 2\frac{\phi\tau x}{V} + (\tau^*\theta)^2 + (\tau\phi)^2. \qquad \text{(A-3)}$$

The θ^2 and ϕ^2 terms are negligible for small angles, so we can ignore these terms and further simplify equation (A-3):

$$t^2 = \left[\tau^* + \tau\right]^2 + \frac{x^2}{V^2} - 2\frac{(\theta\tau^* + \phi\tau)x}{V}. \qquad \text{(A-4)}$$

Notice that equation (A-4) is equivalent to the previously derived equation (1) for a first-order pegleg, with the addition of an offset-dependent correction term for the dipping layers.

Although explicit seabed and subsea reflector dip angles, ϕ and θ, are contained in equation (A-10), they were introduced only to show equivalence to equation (A-4). Locally-planar reflectors are not required to implement equation (3).

Approximation to Levin and Shah's Traveltime Equations for mild reflector dip

In a constant-velocity medium, the expression for x_p derived earlier, equation (4), simplifies to:

$$x_p = \frac{\tau}{\tau + \tau^*} x \tag{A-5}$$

Then $x - x_p$, which will be needed later, simplifies to:

$$x - x_p = \frac{\tau^*}{\tau + \tau^*} x \tag{A-6}$$

Using equations (A-5) and (A-6), we can directly write the (two-way) zero offset traveltime of the seabed and subsea reflection as a function of midpoint location, y_0:

$$\begin{aligned} \tau^*(y_0 - x_p/2) &= \tau^*(y_0) - \frac{x_p \sin\phi}{V} \\ &\approx \tau^*(y_0) - \frac{\phi\ \tau(y_0)\ x}{V(\tau(y_0) + \tau^*(y_0))} \end{aligned} \tag{A-7}$$

$$\begin{aligned} \tau(y_0 - (x - x_p)/2) &= \tau(y_0) - \frac{(x - x_p)\sin\theta}{V} \\ &\approx \tau(y_0) - \frac{\theta\ \tau^*(y_0)\ x}{V(\tau(y_0) + \tau^*(y_0))}, \end{aligned} \tag{A-8}$$

where the small angle approximation was employed as before. Utilizing equations (A-5)-(A-8), we can now manipulate equation (3) to make it resemble Levin and Shah's moveout equation (A-4):

$$t^2 = \left[\tau(y_0) + \tau^*(y_0) - \frac{(\phi\ \tau(y_0) + \theta\ \tau^*(y_0))x}{V(\tau(y_0) + \tau^*(y_0))}\right]^2 + \frac{x^2}{V^2} \tag{A-9}$$

$$\approx \left(\tau(y_0) + \tau^*(y_0)\right)^2 - 2\frac{(\phi\ \tau(y_0) + \theta\ \tau^*(y_0))x}{V} + \frac{x^2}{V^2} \tag{A-10}$$

Equation (A-10) is equivalent to equation (A-4). Therefore, we have proven the equivalence of the moveout equations of the true and approximate raypaths shown in Figure 2, subject to the small dip angle approximation. As before, ϕ^2 and θ^2 terms were dropped in going from equation (A-9) to equation (A-10).

REFERENCES

Brown, M., 2002a, Least-squares joint imaging of primaries and multiples: 72nd Ann. Internat. Mtg., Soc. of Expl. Geophys., Expanded Abstracts, 890–893.

Brown, M., 2002b, Simultaneous estimation of two slopes from seismic data, applied to signal/noise separation: SEP–**112**, 181–194.

Brown, M., 2003a, Amplitude modeling of pegleg multiple reflections: SEP–**113**, 97–106.

Brown, M., 2003b, Least-squares joint imaging of primaries and pegleg multiples: 2-D field data test: SEP–**113**, 17–30.

Fomel, S., 2001, Three-dimensional seismic data regularization: Ph.D. thesis, Stanford University.

Fomel, S., 2002, Applications of plane-wave destruction filters: Applications of plane-wave destruction filters:, Soc. of Expl. Geophys., Geophysics, 1946–1960.

Guitton, A., 2003, Multiple attenuation with multidimensional prediction-error filters: 73rd Ann. Internat. Mtg., Soc. of Expl. Geophys., Expanded Abstracts, submitted.

Levin, F. K., and Shah, P. M., 1977, Peg-leg multiples and dipping reflectors: Geophysics, **42**, no. 05, 957–981.

Lomask, J., and Claerbout, J., 2002, Flattening without picking: SEP–**112**, 141–150.

Morley, L., 1982, Predictive multiple suppression: Ph.D. thesis, Stanford University.

Ross, W. S., Yu, Y., and Gasparotto, F. A., 1999, Traveltime prediction and suppression of 3-D multiples: Geophysics, **64**, no. 1, 261–277.

Verschuur, D. J., Berkhout, A. J., and Wapenaar, C. P. A., 1992, Adaptive surface-related multiple elimination: Geophysics, **57**, no. 09, 1166–1177.

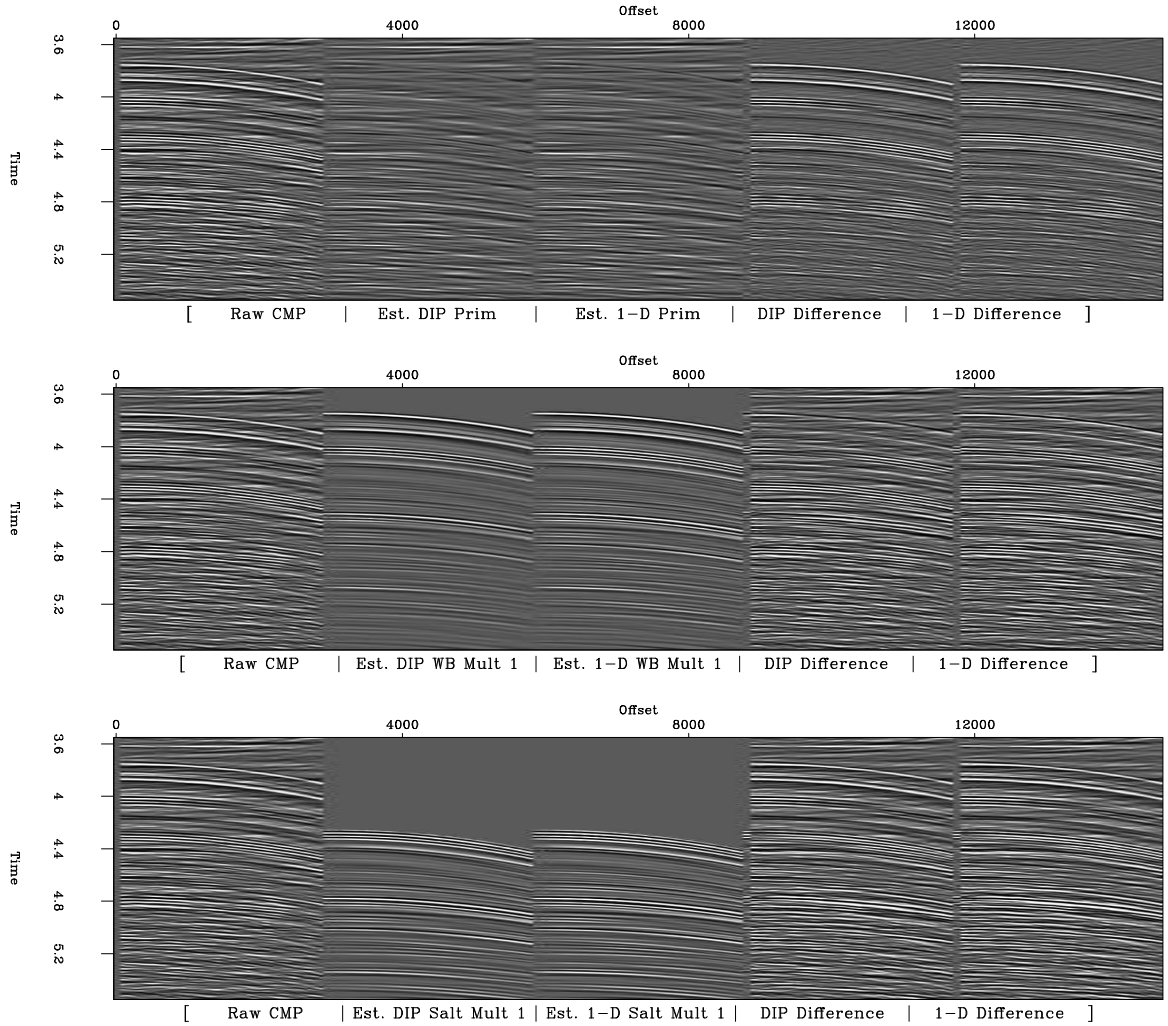

Figure 6: Mississippi Canyon CMP 1 ($y = 0$ m). All panels NMO'ed with stacking velocity and windowed in time from 3.5 to 5.5 seconds. Top row (L to R): Raw data; Estimated HEMNO primaries; Estimated 1-D primaries; HEMNO difference; 1-D difference. Center row (L to R): Raw data; Estimated HEMNO total first order seabed multiple ($\sum_{k=0}^{1} \mathbf{R}_{1,1}\mathbf{N}_{1,k,1}\mathbf{S}_{1,1}\mathbf{G}_{1,1}\mathbf{m}_{1,k,1}$); Estimated 1-D total first order seabed multiple; HEMNO difference; 1-D difference. Bottom row (L to R): Raw data; Estimated HEMNO total first order "salt" (R1 at this location) multiple ($\sum_{k=0}^{1} \mathbf{R}_{1,2}\mathbf{N}_{1,k,2}\mathbf{S}_{1,2}\mathbf{G}_{1,2}\mathbf{m}_{1,k,2}$); Estimated 1-D total first order salt multiple; HEMNO difference; 1-D difference. morgan1-comp1.lsrow.dip-nodip.gulf.0 [CR]

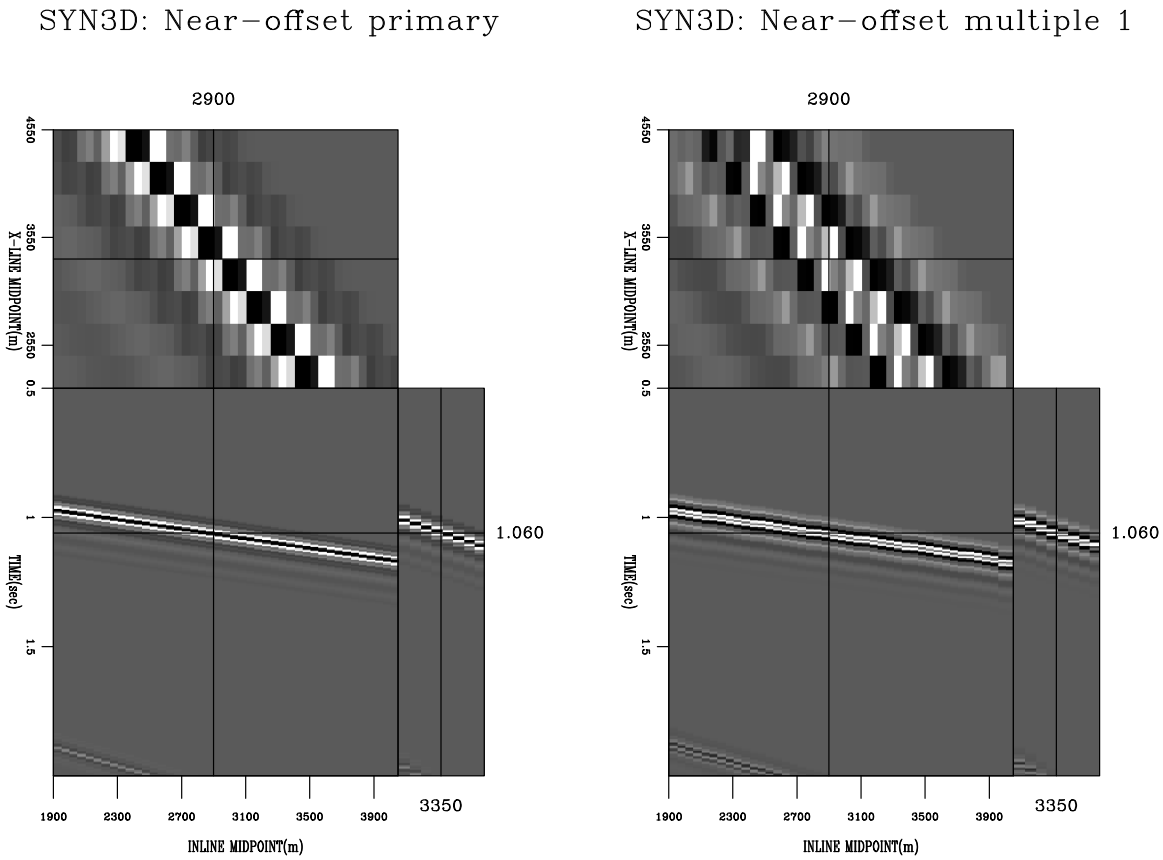

Figure 7: HEMNO demonstration on synthetic 3-D dataset. 8 swaths of 43 shots were acquired over a seabed reflector with 4 degrees of inline dip and 2 degrees of crossline dip. Acquisition was 3 streamers with 300 m crossline separation. Left panel shows the zero offset section after conventional NMO for primaries. Right panel shows zero offset section after HEMNO for multiples. Notice how, over all midpoints, the seabed reflections in each panel are coincident. morgan1-syn3d.comp [CR,M]